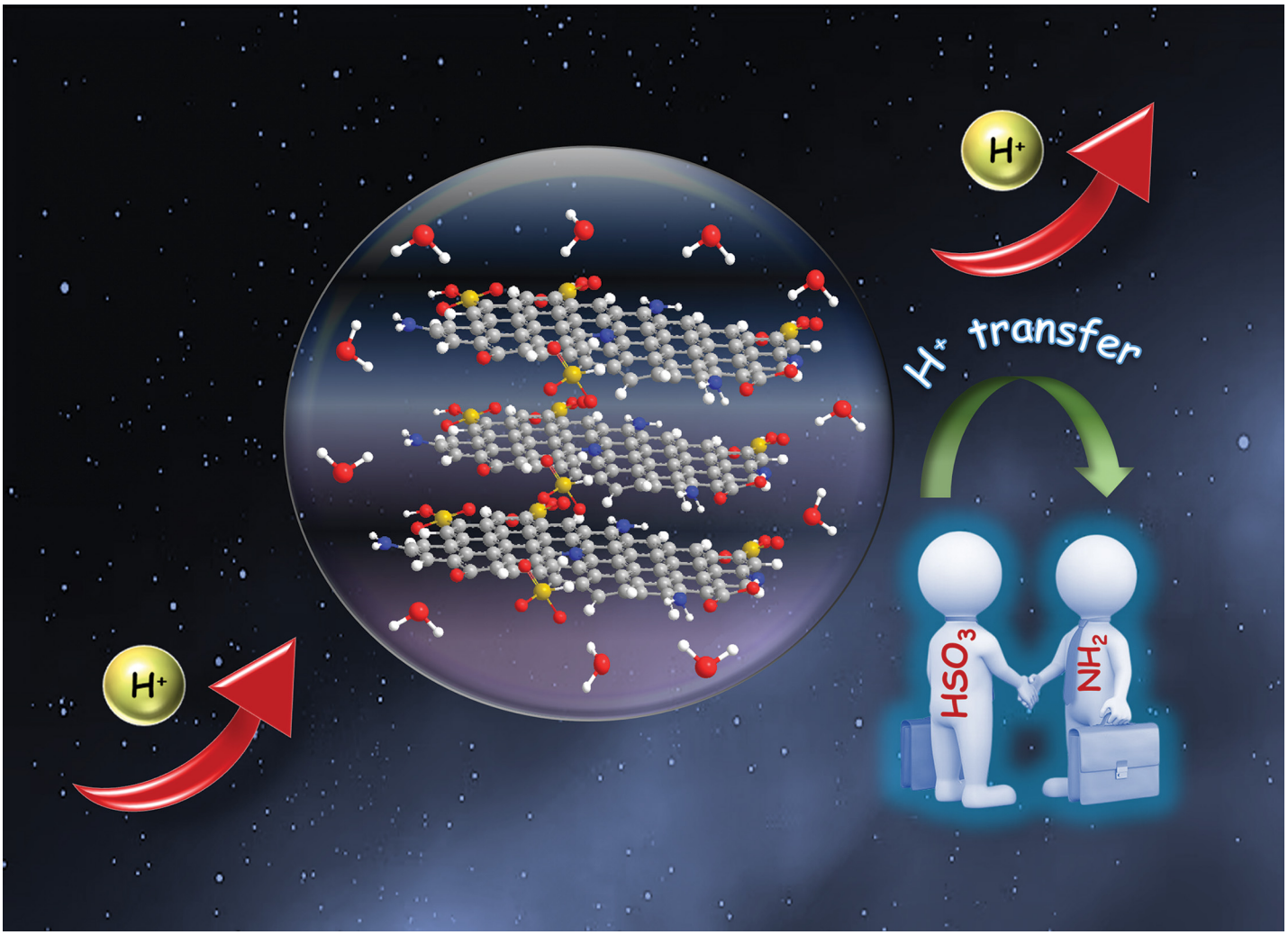

Showcasing research from Professor Amit Paul's laboratory, Department of Chemistry, Indian Institute of Science Education and Research (IISER), Bhopal, Madhya Pradesh, India.

Remarkable solid-state proton conduction in sulfur- and nitrogen-functionalized few-layer graphene

Sulfur- and nitrogen-functionalized few-layer graphene (SNFG) revealed exceptional solid-state proton conductivity (0.0865 S cm^{-1}) due to acid-base synergism and excess charge carrier, comparable to Nafion with remarkable stability over a month.

Image reproduced by permission of Amit Paul from *Chem. Commun.*, 2025, **61**, 7604.

Image designed and illustrated by Sweety Gupta

As featured in:

See Sweety Gupta and Amit Paul, *Chem. Commun.*, 2025, **61**, 7604.

ROYAL SOCIETY OF CHEMISTRY

rsc.li/chemcomm

Registered charity number: 207890

ChemComm

COMMUNICATION

View Article Online
View Journal | View Issue

Cite this: *Chem. Commun.*, 2025, **61**, 7604

Received 28th March 2025,
Accepted 25th April 2025

DOI: 10.1039/d5cc01752a

rsc.li/chemcomm

Remarkable solid-state proton conduction in sulfur- and nitrogen-functionalized few-layer graphene†

Sweety Gupta and Amit Paul *

Sulfur- and nitrogen-functionalized few-layer graphene exhibited remarkable proton conductivity of 0.0865 S cm^{-1} at 95 °C, 95% RH, comparable to Nafion, with a low activation barrier and exceptional stability over a month. The incorporation of sulfonic acid and nitrogen-functionalities resulted in acid–base synergism and excess charge carriers for proton conduction.

With the depletion of fossil fuels, there is a rapid rise in demand for alternative energy resources. In this context, proton exchange membrane fuel cells (PEMFCs) have gained immense attention, providing a cleaner energy source that can be utilized in various energy-related devices.[1] In PEMFCs, one of the most critical parameters is the ability of protons to transport through the membrane. Nafion was considered to be the most promising material for proton-conducting membranes, but its high cost and instability at high temperatures demand an alternative.[2] In the past decade, several porous materials such as metal–organic frameworks (MOFs),[3,4] covalent organic frameworks (COFs)[5,6] and porous organic polymers (POPs)[7] have been explored, showing reasonable proton conductivity (10^{-7}–10^{-3} S cm^{-1}). However, the high synthesis cost of these materials limits their commercial viability. Thus, there is a need for a cost-effective, high-performing material that can be utilized as a proton-conducting membrane.

Recently, graphene-derived materials have been demonstrated as suitable candidates for proton conduction due to their excellent mechanical strength, low cost and easy fabrication process.[8–12] In this regard, Karim *et al.* used graphite oxide (GO) as a proton-conducting material for the first time, which contained hydrophilic groups such as epoxide, hydroxyl, carboxyl, *etc.*, in between the layers, hence facilitating the conduction of protons.[13] However, deterioration of the epoxy group gradually over time compromises its stability. In contrast, graphene was not extensively investigated due to its hydrophobic nature, small interlayer distance and presence of electron density, which prevents protons from propagating through its sheets. To address this problem and following a theoretical study by Geiger and co-workers,[14] our group first investigated oxygen functionalized few-layer graphene (OFG) as a proton conductor, which exhibited decent proton conduction of 8.7×10^{-3} S cm^{-1} at 80 °C and 95% RH, and an activation barrier of 0.24 eV with long-term stability but having significantly high humidity dependence.[15] Thereafter, graphene edges were functionalized with acidic and basic groups, which synergistically improved their performance by reducing the activation barrier to 0.09–0.10 eV in nitrogen- and oxygen-functionalized graphenes (NOFGs). However, these materials displayed relatively low proton conductivities ($3.6–8.7 \times 10^{-3}$ S cm^{-1}) under fully hydrated conditions at 95 °C.[16] Thus, the development of new proton conductors that exhibit very high conductivity along with low activation barriers and exceptional stability requires further exploration.

To address this issue, acids with low pK_a values, such as sulfonic, phosphonic, and carboxylic acids, can be utilized, which can significantly enhance proton mobility, thereby playing a vital role in the improvement of proton conduction.[17–20] Additionally, both acid and basic functionalities help in lowering the activation barrier due to fast protonation and deprotonation processes.[21] Apart from these factors, the stability of the material is also considered one of the crucial parameters for practical application. The above findings prompted us to anticipate that the functionalization of graphene by nitrogen and sulfonic acid groups could significantly improve solid-state proton conduction at both low humidity and varying temperatures. Herein, we report the synthesis of sulfur- and nitrogen-functionalized few-layer graphene (SNFGs), which display a high proton conductivity of 8.65×10^{-2} S cm^{-1} at 95 °C and 95% RH, which is comparable to commercially available Nafion.[22] Furthermore, SNFG exhibited excellent conductivity

Department of Chemistry, Indian Institute of Science Education and Research (IISER), Bhopal, Madhya Pradesh 462066, India. E-mail: apaul@iiserb.ac.in, sweety22@iiserb.ac.in

† Electronic supplementary information (ESI) available: PXRD, TGA, RAMAN, XPS, water sorption analysis results with additional information of all characterization and synthesis details have been provided. See DOI: https://doi.org/10.1039/d5cc01752a

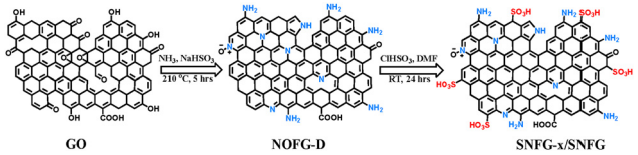

Fig. 1 Scheme of preparation for sulfur- and nitrogen-functionalized few-layer graphene (SNFG).

of 4.61 × 10^{-2} S cm^{-1} at low humidity (40% RH) at 95 °C. The material revealed exceptional stability at 95 °C and 95% RH over a month. In the next few sections, we discuss the synthesis, characterization and proton conduction of SNFG.

The synthesis of SNFG-*x* (wherein *x* represents different amounts of sulfonic acid added during synthesis) has been summarized in Fig. 1, wherein the first step involved the synthesis of graphite oxide (GO) following a modified Hummers' method.[10] The second step involved the synthesis of nitrogen- and oxygen-functionalized graphene (NOFG-D, wherein D denotes direct functionalization of the material from GO) previously reported by us (Fig. 1).[16] In the last step, NOFG-D was treated with different amounts of chlorosulfonic acid to incorporate sulfonic acid functionalities. The complete details of synthesis have been provided in the ESI.† The best material was found to be SNFG-9 based on proton conductivity experiments, and for simplification, we name this material as SNFG only.

FTIR spectra of SNFG revealed stretching bands for NH_2, S═O and C–N at 3400–3300, 1035 and 1170 cm^{-1}, respectively, and these bands were absent in GO (Fig. 2a), confirming the successful incorporation of sulfonic acid and nitrogen functionalities in SNFG. High-resolution XPS spectra of C 1s, O 1s, N 1s and S 2p spectra were recorded and deconvoluted to achieve a deeper understanding of the nature of chemical bonding. C 1s spectra showed five distinct peaks of C═C/C–C, C–OH (hydroxyl), C═O (ketone), C–N and O–C═O (acid), at 284.5, 286.4, 287.9, 285.4 and 288 eV, respectively (Fig. 2b). O 1s spectra revealed three peaks at 531.4 (C═O), 532.7 (S═O) and 534.4 (HO–C═O), respectively, highlighting both oxygen and sulfur containing functionalities (Fig. 2c). The N 1s spectrum exhibited four distinct peaks at 398.6 (pyridinic N), 400.4 (pyrrolic N), 401.4 eV (graphite N) and 402.1 (*N*-oxide) (Fig. 2d)[16] confirming the doping of nitrogen in the graphitic structure. S 2p peaks were deconvoluted into S $2p_{1/2}$ and S $2p_{3/2}$ peaks at 167.6 and 168.7 eV, respectively (Fig. 2e),[23,24] indicating successful incorporation of oxidised sulfur species. Overall XPS demonstrated effective functionalization of both sulfur and nitrogen groups in SNFG showing nitrogen and sulfur content of 5.1% and 0.6%, which was consistent with elemental analysis (CHNS) (Table S1, ESI†).

Powder X-ray diffraction (PXRD) patterns were examined to characterize the structural properties of the materials. 2θ maxima of the (002) plane for GO and SNFG were observed at 10.5° and 24.7°, which correspond to interlayer distances of 8.1 and 3.6 Å, respectively (Fig. S1, ESI†). PXRD peak broadening was observed in SNFG relative to GO, suggesting a significantly reduced crystallite length along the *c*-axis (L_c).[10] Scherrer's formula and Voigt function fitting were employed to calculate the number of layers, revealing approximately five layers in SNFG (see ESI†).[24] These findings suggested a lateral arrangement of four to five graphene nanosheets, exhibiting an interlayer distance of only 3.6 Å due to van der Waals interaction, resulting in the classification of these materials as few-layered graphene.

Another peak also appeared at ~43.3° for the (100) plane. Additional structural features were analysed using Raman spectroscopy, wherein SNFG displayed two prominent peaks at 1346 and 1590 cm^{-1}, which corresponded to the G and D-band, respectively. The D band corresponds to the defects on the graphene sheets, and the G-band corresponds to in-plane vibrations of C atoms. Besides that, three other peaks centred at 2670, 2919, and 3173 cm^{-1} were also observed (Fig. S2, ESI†).[25]

The material's morphology was illustrated from scanning electron microscopy (SEM) and transmission electron microscopy (TEM) images. SEM displayed a well-defined layered structure of SNFG, corroborated by TEM images (Fig. 3a and b). The diffraction spots of the SAED pattern correspond to the hexagonal lattice of the graphene sheets, indicating the crystallinity of the material (Fig. 3b, inset). High-resolution TEM also revealed four to five layers of graphene, with an interlayer spacing of around 3.5 Å, consistent with the PXRD results (Fig. 3c). Besides, elemental mapping showed the uniform distribution of different elements in the structure of graphene (Fig. 3d–g).

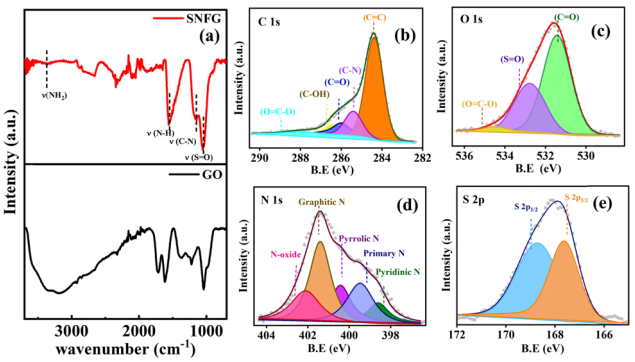

Fig. 2 (a) FTIR spectra of SNFG and GO. XPS of (b) C 1s spectra, (c) O 1s spectra, (d) N 1s spectra and (e) S 2p spectra.

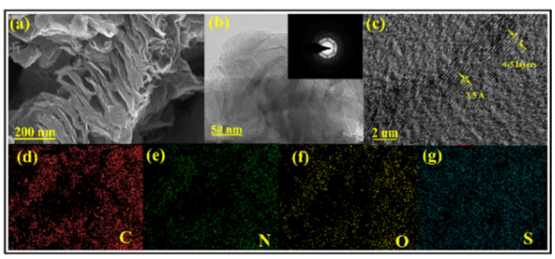

Fig. 3 Microscopic characterizations of SNFG: (a) SEM image, (b) TEM image (inset: SAED pattern), and (c) HRTEM image. (d), (e), (f) and (g) Elemental mapping of carbon, nitrogen, oxygen, and sulfur.

TGA confirmed the thermal stability of SNFG, indicating a minimum weight loss of 3.3% up to 200 °C (loss of labile oxygen functionalities), 6.6% between 200–500 °C (desulfonation),[26] and 8.4% beyond 500 °C (topological defects) (Fig. S3, ESI†).[27] It is important to note that this material was thermally more stable compared to other reported graphene-based materials (Table S6, ESI†).[16] The Brunauer–Emmett–Teller (BET) surface area, pore volume and pore diameter of SNFG were 63 $m^2\ g^{-1}$, 0.1 $cm^3\ g^{-1}$ and 3.8 nm, respectively (Fig. S4, ESI†). The reversible water uptake experiment demonstrated a notable enhancement in water uptake capacities with increasing pressure, achieving maximum uptakes of 328 mL g^{-1} ($n H_2O$) for SNFG at P/P_0 = 0.9 (Fig. S5, ESI†). The room temperature electrical conductivity of the graphene material was found to be 6.6×10^{-2} S cm^{-1} using the two-probe method (Fig. S6, ESI†).

The material was then tested for solid-state proton conduction, employing electrochemical impedance spectroscopy (EIS) at different humidity and temperature conditions. The diameter of the semicircle represents the resistance of proton conduction obtained at the high-frequency region of the Nyquist plot, wherein the imaginary component of impedance (Z'') is plotted against the real component of impedance (Z'). The EIS results were modelled using an equivalent circuit depicted in Fig. S7, ESI† andFig. 4a, b (insets). Subsequently, the proton conductivities (σ_{pc}) were determined using the dimensions of the pelletized sample and the R_{pc} values, following eqn (S5), ESI.† For the fitting of the EIS result, a constant phase element has been employed in place of a capacitor, indicating heterogeneity and surface roughness within the system.[28] At very high frequencies, an inductance contribution was observed in all measurements depicted by L1, which could be associated with external wiring connections of the potentiostat with electrodes (Fig. 4a and b, inset).[29]

First, we measured and compared the proton conductivity of different SNFG materials at 50 °C and 95% RH (Fig. S8, ESI†). Among them, the best material (SNFG/SNFG-9) was used for further temperature dependent proton conduction. Fig. 4a and b represent the Nyquist plots of SNFG at two different relative humidities with variable temperatures. The σ_{pc} values were 1.15×10^{-2} and 4.61×10^{-2} S cm^{-1} at 27 °C and 95 °C at 40% RH, respectively (Fig. 4a and Table S7, ESI†). At 95% RH, the σ_{pc} values increased to 2.75×10^{-2} S cm^{-1} at 27 °C and 8.65×10^{-2} S cm^{-1} at 95 °C, respectively (Fig. 4b and Table S8, ESI†). Thus, at 95 °C and 95% RH, the σ_{pc} values are comparable to that of commercially available Nafion (0.1 S cm^{-1}).[22] These values suggested efficient proton conduction at both humidity conditions, which could be attributed to the presence of highly acidic sulfonic groups ($pK_a \sim -7$)[17] and basic nitrogen groups at the edges of the graphene sheets. To further investigate the proton transport mechanism, the activation energy (E_a) values were determined using the Arrhenius equation (Fig. 4c). The E_a values obtained at 40% and 95% RH values were 0.13 and 0.12 eV, respectively, suggesting that the Grotthuss mechanism was operational in these conditions.

Moreover, experiments were also performed at lower temperatures to ensure that these materials could serve as solid-state proton conductors even at 0 °C. The material showed high proton conductivity of 1.01×10^{-2} at 0 °C at 95% RH. Fascinatingly, the material showed a low activation barrier of 0.18 eV in a wide temperature range of 0 to 95 °C (Fig. S9, ESI†). Thus, it is exciting to note that the material (SNFG) outperformed various graphitic materials substantially compared to various recent literature reports (Table S9b, ESI†). The practical application of proton-conducting materials requires long-term stability. Therefore, time-dependent proton conduction studies were carried out over a month at 95 °C and 95% RH, during which the material showed no decline in its performance (Fig. 4d).

Furthermore, PXRD results confirmed that there was no major alteration of peaks after 30 days in these conditions (Fig. S10, ESI†). Thus, exceptional stability of the material was achieved under high-temperature, high-humidity proton-conducting conditions. Additionally, the thermal robustness of the materials was also checked by heating SNFG at 150 °C for 1 h and its conductivity was measured before and after annealing at 70 °C and 95% RH. The results indicated that thermal annealing did not affect the proton-conductivity of SNFG (Table S10, ESI†). These findings suggest that SNFG exhibits superior proton conduction and is a more suitable option due to its durability.

The detailed mechanism of the proton transport pathways is depicted in Scheme 1, which shows proton migration *via* hydrogen bonding *via* adsorbed water molecules between basic nitrogen functionalities and sulfonic acid located at the edges

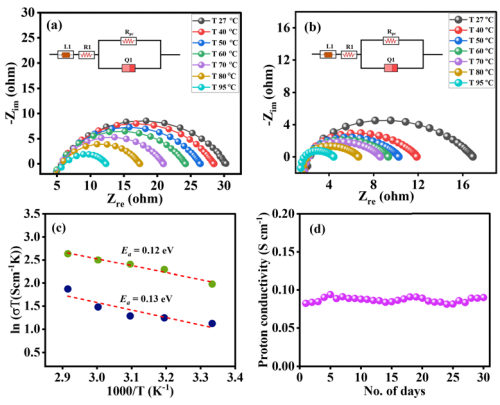

Fig. 4 (a) Nyquist plot of SNFG at 40% and (b) 95% RH, respectively; inset equivalent circuit diagram. (c) Plots of ln(σT) *vs.* T^{-1} at 40% and 95% RH, wherein σ and T are proton conductivity and temperature, respectively. (d) Long term stability test of SNFG-9 at temperature 95 °C and 95% RH.

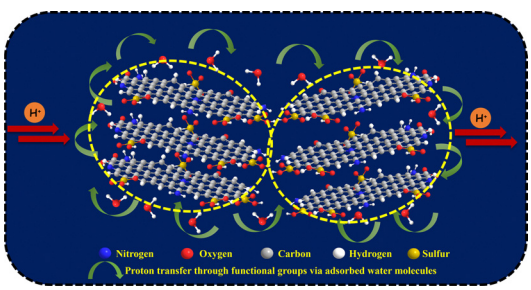

Scheme 1 Proposed mechanisms for proton conductivity through SNFG. Yellow circles represent grain boundary.

of the graphene sheets. Herein, the remarkable proton conductivity of SNFG can be attributed to the introduction of sulfonic acid groups known for their high proton donating ability due to the low pK_a ($\sim(-)7$) to basic nitrogen functionalities (amine, pyridinic, pyrrolic, and graphitic nitrogen). Firstly, these functionalities increased the availability of charge carriers, which helped in improving proton conduction. Secondly, sulfonic acid and various basic nitrogen functionalities provided fast protonation and deprotonation pathways through hydrogen bonding networks of water molecules for efficient proton conduction. The acid–base synergism helped to lower the activation barrier for proton conduction. Thirdly, in solid-state materials, the proton conductivity is represented as $\sigma_{pc} = \sum n \times q \times \mu$, wherein n, q, and μ represent the number of charge carriers, charge possessed by carriers, and their mobility, respectively. Maier and Tuller emphasized that space charge regions at grain boundaries reduce electrostatic energy, hence lowering the barrier resistance.[30,31] Consequently, smaller grain size can markedly improve ion conductivity by increasing the number of charge carriers. In SNFG, the Raman analysis indicated a grain size (L_a) of 7.4 nm (see ESI†), suggesting the presence of a significant number of grain boundaries that can enhance the number of charge carriers. Thus, the structural specifications also contributed to enhanced proton conductivity, while the functionalization facilitated a reduced activation barrier, ensuring reliable performance even at low humidity and across a range of temperatures, including room temperature and lower temperature conditions.

In conclusion, this work summarizes the synthesis of nitrogen- and sulphur-functionalized few-layer graphene (SNFG) as solid-state proton conductors. The incorporation of sulfonic acid and basic nitrogen groups introduced additional charge carriers, which helped in achieving remarkable proton conduction of 8.65×10^{-2} S cm^{-1} at 95 °C and 95% RH, comparable to commercially available Nafion. The synergistic acid–base interactions between sulfonic acid and nitrogen functionalities resulted in fast protonation and deprotonation, which lowered the activation barrier. The smaller grain size of SNFG also helped to enhance the number of charge carriers. It is important to highlight that SNFG displayed excellent proton conduction at a very low temperature (0 °C) and exceptional stability over a month, which should be useful for real-time application. Indeed, the structurally diverse edge-functionalized graphene has the potential to surpass the best proton-conducting material available on the market with significantly better structural stability.

A. P. acknowledges financial support from IISER Bhopal. S. G. acknowledges IISER Bhopal, India, for providing a fellowship. We thank the infrastructural facility provided by IISER Bhopal and FIST-supported TEM facility to the Department of Chemistry, IISER Bhopal.

Data availability

The data supporting this article have been included as part of the ESI.†

Conflicts of interest

There are no conflicts to declare.

References

1 R. Borup, *et al.*, *Chem. Rev.*, 2007, **107**, 3904–3951.
2 Afzal, Y. Ren, S. Wang, H. Ma, S. Yuan, Q. Zhao, M. B. Wadud, X. Liang, Q. Pan, G. He and Z. Jiang, *J. Membr. Sci.*, 2025, **722**, 123863.
3 T. Ren, Y. Liao, M. Wang, J. Hu, Y. Peng and H. Wen, *J. Rare Earths*, 2025, DOI: 10.1016/j.jre.2025.01.009.
4 M. V. Nguyen, H. C. Dong, D. Nguyen-Manh, N. H. Vu, T. T. Trinh and T. B. Phan, *J. Sci.: Adv. Mater. Devices*, 2021, **6**, 509–515.
5 S. Chandra, T. Kundu, S. Kandambeth, R. BabaRao, Y. Marathe, S. M. Kunjir and R. Banerjee, *J. Am. Chem. Soc.*, 2014, **136**, 6570–6573.
6 Z. Meng, A. Aykanat and K. A. Mirica, *Chem. Mater.*, 2019, **31**, 819–825.
7 H. Xu, S. Tao and D. Jiang, *Nat. Mater.*, 2016, **15**, 722–726.
8 P. Mehra, C. Singh, I. Cherian, A. Giri and A. Paul, *ACS Appl. Energy Mater.*, 2021, **4**, 4416–4427.
9 A. Barua, P. Mehra and A. Paul, *ACS Appl. Energy Mater.*, 2021, **4**, 14249–14259.
10 D. Roy Chowdhury, C. Singh and A. Paul, *RSC Adv.*, 2014, **4**, 15138–15145.
11 S. Gupta, P. Mehra and A. Paul, *Sustainable Sci. Technol.*, 2025, **2**, 013001.
12 W. Yang, T. Chen, L. Xie, Y. Yu, M. Long and L. Xu, *Carbon Neutralization*, 2024, **3**, 904–917.
13 M. R. Karim, K. Hatakeyama, T. Matsui, H. Takehira, T. Taniguchi, M. Koinuma, Y. Matsumoto, T. Akutagawa, T. Nakamura, S.-I. Noro, T. Yamada, H. Kitagawa and S. Hayami, *J. Am. Chem. Soc.*, 2013, **135**, 8097–8100.
14 J. L. Achtyl, R. R. Unocic, L. Xu, Y. Cai, M. Raju, W. Zhang, R. L. Sacci, I. V. Vlassiouk, P. F. Fulvio, P. Ganesh, D. J. Wesolowski, S. Dai, A. C. T. van Duin, M. Neurock and F. M. Geiger, *Nat. Commun.*, 2015, **6**, 6539.
15 C. Singh, S. Nikhil, A. Jana, A. K. Mishra and A. Paul, *Chem. Commun.*, 2016, **52**, 12661–12664.
16 P. Mehra, M. Wilson and A. Paul, *J. Phys. Chem. C*, 2022, **126**, 10534–10545.
17 R. Sahoo, S. C. Pal and M. C. Das, *ACS Energy Lett.*, 2022, **7**, 4490–4500.
18 E. K. Kim, S. Son, J. Won, C. K. Kim and Y. S. Kang, *J. Membr. Sci.*, 2010, **348**, 190–196.
19 S. T. Günday, A. Bozkurt, W. H. Meyer and G. Wegner, *J. Polym. Sci., Part B: Polym. Phys.*, 2006, **44**, 3315–3322.
20 Q. Wang, X. Zheng, H. Chen, Z. Shi, H. Tang, P. Gong, L. Guo, M. Li, H. Huang and Z. Liu, *Microporous Mesoporous Mater.*, 2021, **323**, 111199.
21 Y. He, H. Zhang, Y. Li, J. Wang, L. Ma, W. Zhang and J. Liu, *J. Mater. Chem. A*, 2015, **3**, 21832–21841.
22 S. Sasikala, S. V. Selvaganesh, A. K. Sahu, A. Carbone and E. Passalacqua, *J. Membr. Sci.*, 2016, **499**, 503–514.
23 Z. Yang, Z. Yao, G. Li, G. Fang, H. Nie, Z. Liu, X. Zhou, X. A. Chen and S. Huang, *ACS Nano*, 2012, **6**, 205–211.
24 C. Weidenthaler, *Nanoscale*, 2011, **3**, 792–810.
25 A. C. Ferrari, *Solid State Commun.*, 2007, **143**, 47–57.
26 O. A. Knyazheva, O. A. Kokhanovskaya, A. V. Vasilevich, M. V. Trenikhin, A. V. Bukhtiyarov, A. B. Arbuzov, O. N. Baklanova and A. V. Lavrenov, *Thermochim. Acta*, 2023, **728**, 179593.
27 Z.-S. Wu, W. Ren, L. Gao, J. Zhao, Z. Chen, B. Liu, D. Tang, B. Yu, C. Jiang and H.-M. Cheng, *ACS Nano*, 2009, **3**, 411–417.
28 C. Klumpen, S. Winterstein, G. Papastavrou and J. Senker, *J. Mater. Chem. A*, 2018, **6**, 21542–21549.
29 T. Soboleva, Z. Xie, Z. Shi, E. Tsang, T. Navessin and S. Holdcroft, *J. Electroanal. Chem.*, 2008, **622**, 145–152.
30 J. Maier, *Prog. Solid State Chem.*, 1995, **23**, 171–263.
31 H. L. Tuller, *Solid State Ion*, 2000, **131**, 143–157.